LAWRENCE
LIVERMORE
NATIONAL
LABORATORY

LLNL-TR-704341

Viscous Particle Breakup within a Cooling Nuclear Fireball

J. T. Wilkinson, K. B. Knight, Z. Dai, C. E. Ramon, J. D. Reid

October 4, 2016

Disclaimer

This document was prepared as an account of work sponsored by an agency of the United States government. Neither the United States government nor Lawrence Livermore National Security, LLC, nor any of their employees makes any warranty, expressed or implied, or assumes any legal liability or responsibility for the accuracy, completeness, or usefulness of any information, apparatus, product, or process disclosed, or represents that its use would not infringe privately owned rights. Reference herein to any specific commercial product, process, or service by trade name, trademark, manufacturer, or otherwise does not necessarily constitute or imply its endorsement, recommendation, or favoring by the United States government or Lawrence Livermore National Security, LLC. The views and opinions of authors expressed herein do not necessarily state or reflect those of the United States government or Lawrence Livermore National Security, LLC, and shall not be used for advertising or product endorsement purposes.

This work performed under the auspices of the U.S. Department of Energy by Lawrence Livermore National Laboratory under Contract DE-AC52-07NA27344.

Viscous Particle Breakup within a Cooling Nuclear Fireball

J.T. Wilkinson[1,2], K.B. Knight[2], Z. Dai[2], C.E. Ramon[2], J.D. Reid[1]

[1]Lock Haven University of Pennsylvania
[2]Lawrence Livermore National Laboratory

Abstract

Following the surface detonation of a nuclear weapon, the Earth's crust and immediate surroundings are drawn into the fireball and form melts. Fallout is formed as these melts incorporate radioactive material from the bomb vapor and cool rapidly. The resultant fallout plume and dispersion of radioactive contamination is a function of several factors including weather patterns and fallout particle shapes and size distributions. Accurate modeling of the size distributions of fallout forms an important data point for dispersion codes that calculate the aerial distribution of fallout. While morphological evidence for aggregation of molten droplets is well-documented in fallout glass populations, the breakup of these molten droplets has not been similarly studied. This study documents evidence that quenched fallout populations preserve evidence of molten breakup mechanisms.

Introduction

Fallout is created when a nuclear device is detonated near the Earth's surface. The ensuing fireball can reach millions of degrees, vaporize surrounding material and, if close enough to the surface, melt surface materials like silicate soils[1]. During the turbulent mixing of the fireball, entrained molten silica is shaped by the shear forces and the viscosity of the liquid. This, in turn, affects the population of particle sizes as well as subsequent transport properties. Smaller particles are suspended in the atmosphere for longer periods of time and can therefore be transported farther. An accurate understanding of particle size distribution can improve modeling of fallout contamination needed to guide the movements of people or machinery into, through, or evacuation out of hazardous areas. Evidence for particle agglomeration exists[2], but this study focuses on the less well-studied process of silicate particle breakup, and how breakup may impact the resultant size distribution of fallout. This study searched for definitive evidence of particle breakup mechanisms within glassy fallout.

Samples and Methods

Analysis of particle breakup focused on a selection of elongated samples of glassy fallout originating from a historical U.S. test. Initial selection was produced from four sieve sizes (1.7, 2.0, and 2.4 mm) and consisted of 24 particles (Fig. 1), with the aim of finding glasses representing objects quenched in the process of breakup. Initial sample selection was based on distortion from an ideally spherical particle. Physical attributes such as the degree of particle elongation, and symmetry along the primary axis were key criteria suggesting rotational motion, and initiation of breakup.

Figure 1. Optical images showing the array of elongated morphologies that may preserve evidence of breakup mechanisms.

The 24 glass pieces were optically imaged (see Appendix) to refine the selection based on morphological features. Larger particles tended to be made up of multiple agglomerated pieces, and were therefore discarded to focus on simplified samples that might preserve breakup textures. Dumbbell-shaped particles were singled out because they represent fragile samples

approaching the breaking point. Ellipsoid particles were also chosen as possible precursors preserving initial deformity from an ideally spherical particle. A few samples demonstrated stretched central regions, suggesting that they may be an intermediate texture.

Following sample selection, a subset of 21 samples were coated in carbon (which prevents charging), and characterized using an FEI Inspect F scanning electron microscope (SEM) equipped with an Everhart-Thornley secondary-electron (SE) detector, a solid state diode backscattered-electron (BSE) detector. SE imaging brings out morphological features of sample surfaces, while BSE images contrast differing proton dense regions with other areas of the sample providing a qualitative image of the relative average composition of the sample. Imaging the sample surfaces allowed for the further refining of the sample set. Surfaces with stretched regions were kept, and an array of elongation morphologies were chosen. Samples consisting of multiple agglomerated particles were excluded.

16 of these samples were mounted into a set of two 2.54 cm diameter stainless steel disks drilled with wells sufficient to accommodate each piece. The disks were polished to an approximate mid-section, to a 1 μm finish, and carbon coated for conductivity. Samples were characterized by EDS near the central pinch points to semi-quantitatively determine the major element compositions. Samples were also later quantitatively mapped using element-specific X-rays. Both sets of analyses used the Bruker XFlash 6160 X-ray detector on the FEI Inspect F SEM to perform X-ray energy dispersive spectroscopy (EDS).

Deformation Characterization

Prior to mounting and polishing the samples, the physical dimensions of each piece were recorded. The length, L, and breadth, B, of the sample were measured to calculate the deformation parameter that describes the degree of droplet deformation from an ideally spherical particle.

Sample	Length	Breadth	D
NT-2-10-2	5.38	2.14	0.43
NT-2-14-2	4.06	1.49	0.46
NT-2-14-4	3.67	1.22	0.50
NT-2-12-3	5.08	1.43	0.56
NT-2-12-9	4.38	1.24	0.56
NT-2-12-7	4.9	1.33	0.57
NT-2-12-2	4.98	1.19	0.61
NT-2-14-5	3.75	0.83	0.64
NT-2-14-7	4.38	0.94	0.65
NT-2-12-10	5.85	0.92	0.73
NT-2-10-7	8.3	1.18	0.75
NT-2-12-5	7.92	1.15	0.75
NT-2-14-6	5.11	0.69	0.76
NT-2-12-4	6.45	0.82	0.77
NT-2-10-1	6.43	0.79	0.78
NT-2-10-3	8.68	1.04	0.79
NT-2-10-5	8.82	1.05	0.79
NT-2-14-3	6.62	0.78	0.79
NT-2-12-1	5.74	0.52	0.83
NT-2-10-4	7.77	0.68	0.84
NT-2-14-1	6.1	0.39	0.88

Table 1. Deformation parameter D measured for the sample set. Values around 0.5 represent a short ellipsoid. Higher values tend to reflect elongate samples with a narrow neck, and were likely quenched prior to breakup.

Deformation, D, is calculated as $D = \frac{L-B}{L+B}$. Limits of this parameter are D=0, a sphere, and D=1, a long thin rod[3]. This parameter is useful because experimental studies of breakup of viscous fluids describe D = 0.5 to be the upper limit for particle stability[4]. Values higher than this limit generally lead to breakup after sufficient time. Nearly every particle characterized was above this

threshold (see Table 1), but quenched prior to breakup.

Characterization of Viscosity

In a fireball, cooling to below molten silicate quench temperatures (*e.g.*, ~1400 K[5]) occurs over seconds for most yields[1]. At lower temperatures, viscosity becomes a significant factor impeding the potential breakup of molten materials[2]. A major control on viscosity in molten silicates is chemical composition.

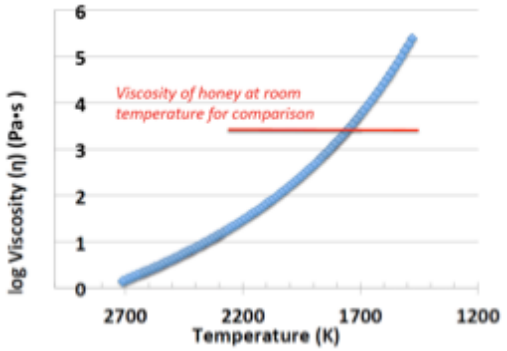

Figure 2. Viscosity curve (see ref. 7) showing how the viscosity of molten glass increases with fireball cooling. The y-axis is logarithmic.

The parameter of viscosity was constrained by analyzing the composition of these types of glass. Compositional data from over 800 locations within related samples[6] were compiled to establish average oxide composition of the glassy fallout. A viscosity calculator[7] that was experimentally determined by Giordano *et al.* (2008) was utilized to create a viscosity curve as a function of temperature. In this calculator, the equation $\log \eta = A + \frac{B}{T(K)-C}$ combines coefficients B and C, which are weighted averages of multi-elemental compositions, with the temperature (T) and a constant, A, which is an empirically determined high temperature limit of viscosities with value -4.55 (representing the viscosity that all liquids approach at infinite temperature). Eta, η, is the viscosity. The resultant curve (Fig. 2) shows that viscosity ranges over 5 orders of magnitude for the temperature range of the cooling fireball.

Compositional Evidence of a Sole Precursor

Of concern was whether or not the selection of samples represented single molten precursors breaking apart, or aggregated materials preserving some cohesion. Colliding particles with enough momentum at the proper incident angle will break apart[8], but for these analyses a simple, single particle origin was desired. Previous studies have shown that agglomerated samples are not well-mixed over these time scales, and samples tend to preserve some composition evidence[9].

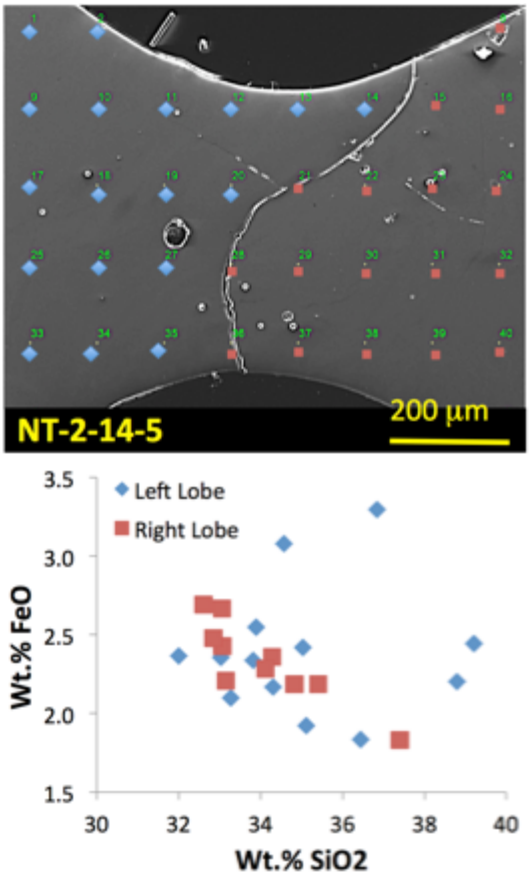

Figure 3. Location of analytical data (top) collected by EDS near the pinch point of sample NT-2-14-5. The central region was analyzed for composition at regularly spaced intervals. The crack in the sample divides the left and right lobes (shown in blue and red respectively), and analyses on the crack were excluded from the comparison. The iron oxide compositions were plotted (bottom) as a function of the silicon dioxide weight percent for each spot analysis. The spread shows variation but considerable overlap.

Data from both lobes of the particle were compared under the assumption that demonstration of compositional heterogeneity supports an origin for the morphology as deriving from a single host particle precursor. The average major element composition (as oxides) from each lobe, and their standard deviations were compared (see Fig. 3). Si, Ca, K, Na, Ti, Fe, and Al were the eight elements compared in an ANOVA test for significance. This test compared the two data sets from each lobe and determined single particle deformation with 95% confidence for positive results. Most of the analyzed particles were confirmed to compositionally support a single particle origin (see Table 2). The table lists the mean and standard deviations for the left and right lobes of the samples. F-test values greater than the significance threshold of 0.05 support the null hypothesis.

Compositional Mapping of Flow Textures

Like viscosity, the influence of internal circulation on particle breakup is also related to the ability of the fluid to flow. While shear forces within the cooling fireball in competition with viscous forces of the individual particles are the likely predominant cause for single particle breakup, an opposing internal circulation within single objects is thought to stabilize the neck of the particle[10]. Pinching of the central region becomes more prominent and the deformation parameter increases if circulation is not present. A subset of samples where therefore selected to be polished so that compositional evidence of flow could be looked for.

To more closely examine the compositional textures at the pinch points of these samples, the polished mounts were placed within the SEM to produce qualitative X-ray elemental maps. A total of 6 samples were mapped in the SEM for 16 hours at 75X magnification, with a spot size of 5.5 and an accelerating voltage of 20kV. Si, O, Ca, Mg, K, Na, Ti, Fe, and Al were the focus of compositional mapping because, based on prior EDS analyses, they had been shown to be the main constituents. Aluminum, the most abundant element after Si and O, showed excellent compositional contrast, and proved to be a good indicator of internal flow.

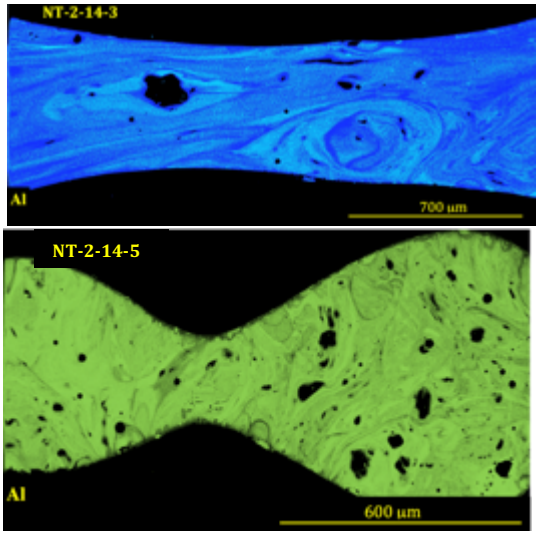

Figure 4. Al X-ray maps from the sample suite. Aluminum is a major element in these samples, and best captured internal compositional textures. Maps have been adjusted to maximize contrast variation in aluminum concentration. Of note, sample NT-2-14-3 (in blue) shows aluminum concentrations within the elongated sample where flow between the lobes is evident. NT-2-14-5 (in green) shows a more tightly pinched join, with little flow present along the narrowed neck.

Figure 5 illustrates the full range of compositional textures observed. Of note, evidence of fluid movement between the lobes is present in the central region of NT-2-14-3, and likely stabilized this sample from pinching to the point of failure. As the fireball environment is thermally heterogeneous, this sample could also have existed in a hotter, less viscous environment prior to quenching, which would have provided additional stability to the droplet. NT-2-12-5, by comparison, is much shorter in length than NT-2-14-3 (3.75 mm vs. 6.62 mm). NT-2-14-5 has a lower deformation parameter (D=0.64 vs. D=0.79; Table 1), but evidence of significant flow along the sample axis is absent. This may indicate

cooler, more viscous conditions served to prevent break apart prior to quenching in this sample.

Discussion

Several competing forces can affect droplet deformation and breakup. Molten particle deformation and breakup have been studied in shear fields (see references 3,5), and analogies can be made to turbulent flow environments that may more realistically represent fireball conditions. Although laminar shear flows are relatively stable, dynamic flow effects will promote breakup[5]. Surface tension is another (temperature dependent) force that impacts the probability for droplet breakup, as does internal flow.

Internal circulation of fluid is thought to stabilize ellipsoidal shapes[3]. If no internal circulation exists, pinching resulting from elongation is not opposed and will proceed more rapidly. Droplets with a larger radius will deform more easily because cohesive forces decrease for larger particles. Although the deformation parameter is a simple comparison between length and breadth, particles with similar values may be proportionally larger or smaller. Taking this into account, elongation and thinning at the neck increase fragility and could play a proportionally larger role in larger particles. The role of internal circulation is thought to stabilize the particle but turbulent and shear forces will likely overcome that in time. Circulation may have only slowed breakup and allowed quenching to occur prior to breakup, but there is ample evidence to support particle breakup within a fireball environment.

Other second order forces affecting particle breakup include a surface tension gradient, with the higher tension existing at the ends. Also, due to particle rotation, centripetal acceleration exists, and results in a pressure gradient (Fig. 5) of decreasing pressure in the direction of the acceleration.

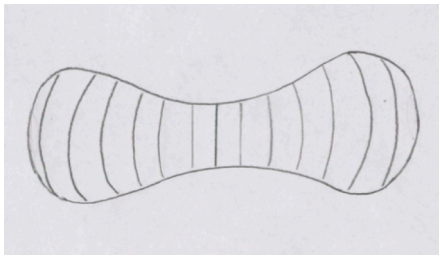

Figure 5. A theoretical pressure gradient within the sample is drawn. As distance from the axis of rotation increases, pressure will also increase. The diagram showcases a particle spinning about the central axis.

These gradients may influence internal buoyant forces. Finally, the presence of bubbles (rounded black voids in the images above) may decrease particle stability. Gaseous inclusions and circulation (best seen in compositional maps, Fig. 4) can also affect the probability of break up.

Conclusions

Particles within a fireball have a turbulent history. We confirm that resultant fallout preserves physical and chemical attributes that show particle breakup does occur, and the studied samples all appear to have been quenched at varying stages of breakup. Mapping of single elements gave the best indications of internal flow, where present. Major element variations reveal compositional diversity, and compositional textures suggest that breakup was on-going, prior to quenching. These maps also support the importance of internal material flow in opposing deformation and breakup. As the fireball cools to a vapor, mechanical deformation can occur, and viscosity and shear rate become dominating factors[1] affecting breakup probability. Particle stability is a balance of forces, but once deformation reaches a threshold, shear forces can overcome surface tension and cohesive forces, tearing the particle apart. The degree to which this balance of forces promotes or hinders breakup may be modeled in future work.

Acknowledgments

I would like to thank my co-authors, as well as Marc Fitzgerald, Laurence Lewis, and David Weisz for their assistance and

suggestions in my research. This work was performed under the auspices of the U.S. Department of Energy by Lawrence Livermore National Laboratory under Contract DE-AC52-07NA27344.
We thank the U.S. Department of Energy's National Nuclear Security Administration, Office of Defense Nuclear Nonproliferation Research and Development, for financial support. LLNL-TR-704341.

References

1 Glasstone, S., & Dolan, P.J. (1977). The Effects of Nuclear Weapons. US Department of Defense; US Department of Energy
2 Weisz, D.G. (2016). Mass Transport of Condensed Species in Aerodynamic Fallout Glass from a Near-Surface Nuclear Test. UC Berkeley Thesis.
3 Karam, H.J., & Bellinger, J.C.(1968). Deformation and Breakup of Liquid Droplets in a Simple Shear Field. Industrial & Engineering Chemistry Fundamentals. 7(4). 576-581.
4 Stone, H.A. (1994). Dynamics of Drop Deformation and Breakup in Viscous Fluids. Annual Review of Fluid Mechanics. 26. 65-102.
5 Cassata, W.S., Prussin, S.G., Knight, K.B., Hutcheon, I.D., Isselhardt, B. H., & Renne, P.R. (2004). When the dust settles: stable xenon isotope constraints on the formation of nuclear fallout. Journal of Environmental Radioactivity. 137. 88-95.
6 L. Lewis, pers. comm.
7 Giordano, D., Russell, J.K., Dingwell, D.B. (2008). Viscosity of Magmatic Liquids. Earth and Planetary Science Letters. 271. 123-134.
8 Qian, J., Law, C.K. (1997). Regimes of coalescence and separation in droplet collision. Journal of Fluid Mechanics. 331. 59-80.
9 Lewis, L.A. et al. (2015). Spatially-resolved analyses of aerodynamic fallout from a uranium-fueled nuclear test. Journal of Environmental Radioactivity. 148. 183-195.
10 Rallison, J.M. (1984). The Deformation of Small Viscous Drops and Bubbles in Shear Flows. Annual Review of Fluid Mechanics. 16. 45-66.

Sample	Lobe	Spots		Na	Al	Si	K	Ca	Ti	Fe
NT-2-12-1	Left	14	Mean	1.30	7.02	32.76	2.83	1.20	0.23	2.25
			Std. Deviation	0.14	0.40	1.21	0.11	0.12	0.03	0.14
	Right	12	Mean	1.29	7.20	33.35	2.75	1.39	0.21	2.24
			Std. Deviation	0.14	0.32	0.68	0.17	0.29	0.04	0.13
			f -test value	0.92	0.44	0.05	0.12	0.01	0.78	0.87
NT-2-12-4	Left	13	Mean	1.55	6.68	33.21	2.95	1.09	0.24	2.10
			Std. Deviation	0.31	1.06	2.33	0.34	0.26	0.03	0.30
	Right	12	Mean	0.89	3.68	16.88	1.49	0.68	0.25	1.29
			Std. Deviation	0.65	3.57	17.44	1.47	0.61	0.27	1.06
			f -test value	0.32	0.06	0.76	0.00	0.49	0.38	0.06
NT-2-14-2	Left	23	Mean	2.06	7.27	32.87	3.50	2.35	0.23	2.16
			Std. Deviation	0.54	1.11	3.76	0.75	1.00	0.04	0.41
	Right	23	Mean	1.79	6.66	33.52	3.20	1.83	0.27	2.20
			Std. Deviation	0.31	1.27	3.76	0.83	0.71	0.10	0.34
			f -test value	0.05	0.29	0.69	0.42	0.18	0.00	0.03
NT-2-14-3	Left	15	Mean	0.87	3.34	15.18	1.47	0.86	0.22	1.11
			Std. Deviation	0.64	3.01	14.91	1.32	0.67	0.20	0.91
	Right	14	Mean	0.83	3.07	13.89	1.39	0.84	0.22	1.02
			Std. Deviation	0.63	2.82	14.07	1.24	0.66	0.20	0.86
			f -test value	0.90	0.65	0.81	0.64	0.81	0.83	0.99
NT-2-14-4	Left	16	Mean	1.50	7.88	32.15	2.85	0.93	0.32	2.63
			Std. Deviation	0.25	1.12	3.01	0.24	0.18	0.09	0.58
	Right	21	Mean	1.53	7.01	33.01	2.83	0.93	0.26	2.15
			Std. Deviation	0.22	1.03	1.83	0.16	0.20	0.08	0.27
			f -test value	1.00	0.53	0.05	0.39	0.81	0.64	0.00
NT-2-14-5	Left	16	Mean	1.42	6.46	35.10	2.85	1.44	0.16	2.39
			Std. Deviation	0.36	0.60	2.18	0.32	0.58	0.04	0.41
	Right	10	Mean	1.19	6.84	34.07	2.85	1.04	0.17	1.02
			Std. Deviation	0.20	0.50	1.49	0.22	0.30	0.06	0.87
			f -test value	0.08	0.58	0.26	0.28	0.06	0.26	0.16
NT-2-14-7	Left	20	Mean	0.84	3.23	14.49	1.42	0.81	0.24	1.10
			Std. Deviation	0.58	2.80	13.43	1.16	0.58	0.22	0.86
	Right	13	Mean	0.78	3.02	13.27	1.25	0.67	0.26	1.03
			Std. Deviation	0.53	2.94	14.87	1.17	0.40	0.23	0.85
			f -test value	0.06	0.79	0.95	0.62	0.34	0.29	0.72

Table 2. ANOVA Test Values

The above table shows the means and standard deviations for the left and right lobes of the listed samples. The f-test was the statistical method used which compared the average and spread of two ranges of data. The test had a significance threshold at 0.05, therefore values below this are considered different and have less than a 95% confidence.

Appendix

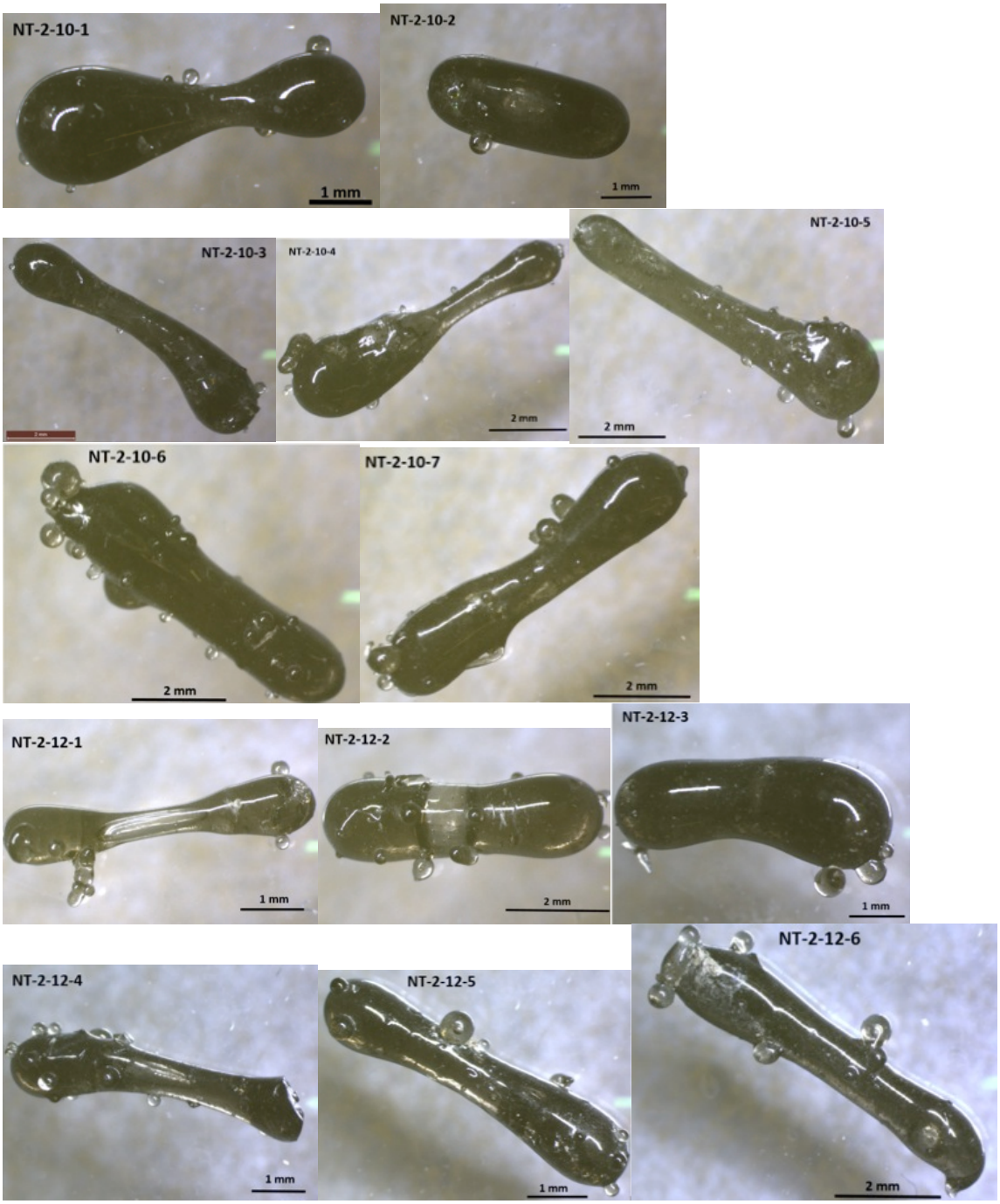
NT-2-10-1
1 mm
NT-2-10-2
1 mm
NT-2-10-3
NT-2-10-4
2 mm
NT-2-10-5
2 mm
NT-2-10-6
2 mm
NT-2-10-7
2 mm
NT-2-12-1
1 mm
NT-2-12-2
2 mm
NT-2-12-3
1 mm
NT-2-12-4
1 mm
NT-2-12-5
1 mm
NT-2-12-6
2 mm

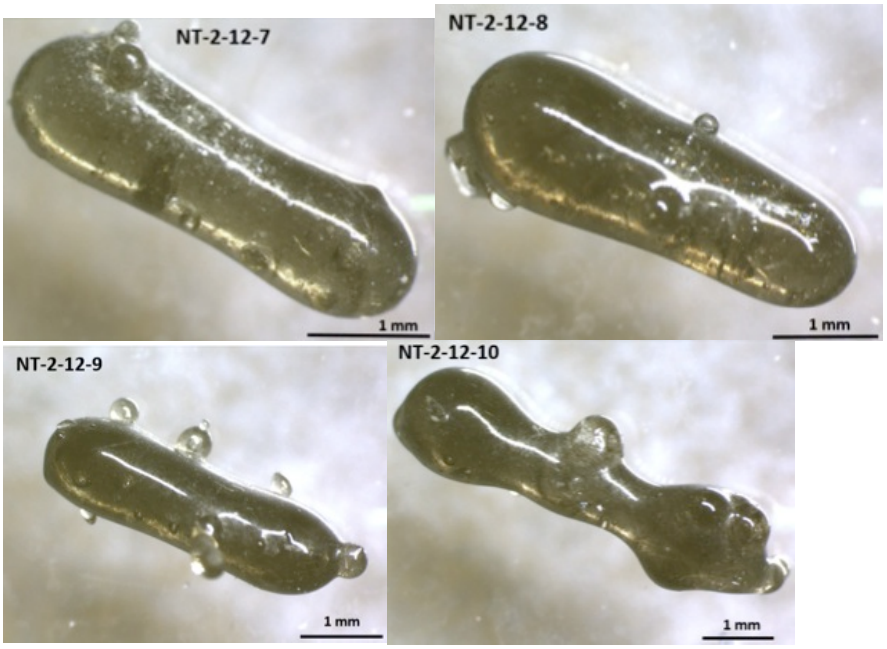

Figure A1. Optical photos from the original sample selection. A variety of morphologies are present.